Author(s): Savin, Hele & Repo, Päivikki & von Gastrow, Guillaume & Ortega, Pablo & Calle, Eric & Garín, Moises & Alcubilla, Ramon

Title: Black silicon solar cells with interdigitated back-contacts achieve 22.1% efficiency

Year: 2015

Version: Post print

Please cite the original version:

Savin, Hele & Repo, Päivikki & von Gastrow, Guillaume & Ortega, Pablo & Calle, Eric & Garín, Moises & Alcubilla, Ramon. 2015. Black silicon solar cells with interdigitated back-contacts achieve 22.1% efficiency. Nature Nanotechnology. 11. DOI: 10.1038/nnano.2015.89.

ARTICLES
PUBLISHED ONLINE: 18 MAY 2015 | DOI: 10.1038/NNANO.2015.89
nature nanotechnology

Black silicon solar cells with interdigitated back-contacts achieve 22.1% efficiency

Hele Savin[1]*, Päivikki Repo[1], Guillaume von Gastrow[1], Pablo Ortega[2], Eric Calle[2], Moises Garín[2] and Ramon Alcubilla[2]

The nanostructuring of silicon surfaces—known as black silicon—is a promising approach to eliminate front-surface reflection in photovoltaic devices without the need for a conventional antireflection coating. This might lead to both an increase in efficiency and a reduction in the manufacturing costs of solar cells. However, all previous attempts to integrate black silicon into solar cells have resulted in cell efficiencies well below 20% due to the increased charge carrier recombination at the nanostructured surface. Here, we show that a conformal alumina film can solve the issue of surface recombination in black silicon solar cells by providing excellent chemical and electrical passivation. We demonstrate that efficiencies above 22% can be reached, even in thick interdigitated back-contacted cells, where carrier transport is very sensitive to front surface passivation. This means that the surface recombination issue has truly been solved and black silicon solar cells have real potential for industrial production. Furthermore, we show that the use of black silicon can result in a 3% increase in daily energy production when compared with a reference cell with the same efficiency, due to its better angular acceptance.

Black silicon (b-Si)—as its name implies—absorbs light very efficiently for a wide range of wavelengths and, as a result, appears black to the naked eye. Its high absorption is based on gradual matching of the refractive index at the silicon/air interface using small nanostructures with dimensions below the wavelength of the incident light[1]. Various shapes (including nanocones[2], nanowires[3], microwires[4] and porous silicon[5]) have been used to achieve excellent light management effects. Because of its many superior properties, b-Si has potential for a range of applications, such as self-cleaning surfaces[6], microelectromechanical systems[7], ion mobility spectrometers[8], terahertz emitters[9], drug analysis[10], photodetectors[11] and antibacterial surfaces[12].

Black silicon would also appear to be an ideal material for photovoltaics due to its outstanding light management properties under the solar spectrum. In addition to boosting efficiency, b-Si can provide significant savings in manufacturing costs as there is no need to deposit a separate antireflection coating. The main challenges that have hindered the use of b-Si in photovoltaics are related to increased surface recombination due to the larger surface area of the nanostructures, and the situation is even more challenging in a conventional front-contacted solar cell structure due to Auger recombination at these highly doped nanostructures[5]. This means that a high number of light-generated electron–hole pairs are lost in the nanostructures instead of being collected at the contacts, reducing the efficiency. Auger recombination can be avoided by using an interdigitated back contact (IBC) solar cell design where the junction and the contacts are placed at the back of the cell[13], but the recombination problem due to the larger surface area remains unsolved. To date, the surface passivation issue has generally been addressed by rather conventional methods, such as depositing silicon nitride by means of plasma-enhanced chemical vapour deposition[14] or with thermally grown silicon dioxide[15], resulting in tradeoffs between reflectance and recombination. The final efficiency has therefore been limited by recombination at the increased b-Si surface, and the reported efficiencies have remained well below 20% (18.2% with a surface area of 0.8 cm^2)[5]. However, our preliminary experiments on pin-hole-free and highly conformal atomic layer deposited (ALD) thin films combined with the chemical and field-effect passivation ability of Al_2O_3 (ref. 16) have shown promising results in overcoming the problematic surface recombination issue in b-Si[17]. Minority carrier lifetimes in the millisecond range indicate excellent surface passivation of b-Si and are in the range needed for high-efficiency solar cells (>20%)[17,18].

Previous b-Si solar cell results have been limited to those from conventional front-side aluminium back surface field (Al-BSF) structures or ultrathin back-contacted cells[13], probably because these structures are less sensitive to front surface recombination. Here, we study the potential of ALD Al_2O_3 passivated b-Si to address the above-mentioned surface recombination problem present in nanostructured surfaces. We select a solar cell design that is known to be extremely sensitive to surface recombination—a thick interdigitated back-contact back-junction (IBC) solar cell[19]. In IBC cells, a majority of the photogenerated charge carriers have to diffuse a long distance from the front surface to the back side of the cells. A thick IBC cell is thus a very demanding structure even for conventionally textured solar cells. If b-Si works in this highly demanding structure, then the surface recombination challenge can be considered solved and b-Si should also be applicable to other cell structures.

Reflectance and surface recombination

Different methods for fabricating b-Si have been introduced, such as laser texturization[20], plasma immersion ion implantation[14] or metal-assisted wet etching[21]. Here, we use cryogenic deep reactive ion etching (DRIE) as it has multiple advantages: it is fast and inexpensive, there is no dependence on crystalline orientation, and there is no requirement for mask layers[22]. As can be seen in Fig. 1a, etching results in random nanoscale structures with a typical height of ~800 nm and width of 200 nm. A precise description of

[1]Department of Micro and Nanosciences, Aalto University, Tietotie 3, Espoo 02150, Finland. [2]Departament d'Enginyeria Electrònica, Universitat Politècnica de Catalunya, Jordi Girona 1-3, Mòdul C4, Barcelona 08034, Spain. *e-mail: hele.savin@aalto.fi

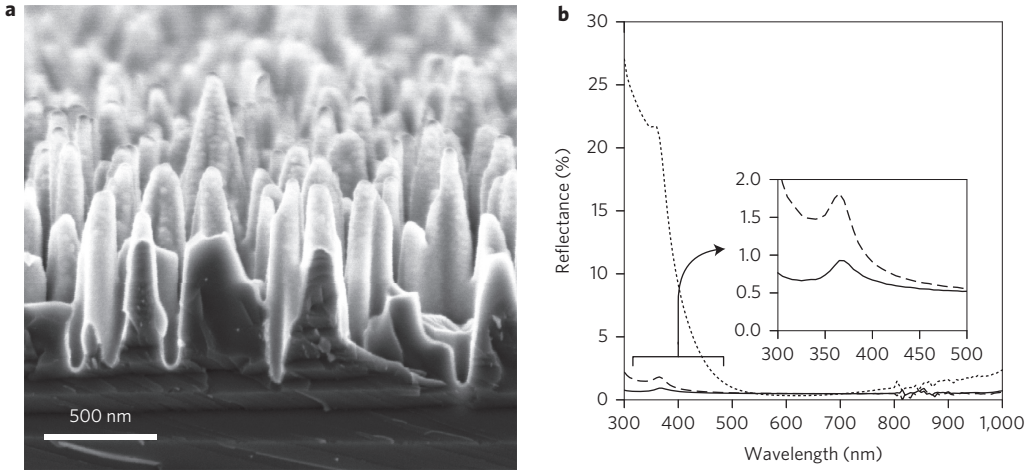

Figure 1 | Structure and reflectance of b-Si. a, Scanning electron microscopy (SEM) image (cross-sectional view) of a b-Si surface. Typical height of a silicon pillar, ~800 nm; diameter at the bottom of the pillar, ~200 nm. The 20 nm Al_2O_3 layer can be seen as a brighter layer on top of the pillars. **b**, Measured reflectance spectra in the 300–1,000 nm wavelength range. The dashed line represents the reflectance of a bare b-Si sample and the black solid line shows the reflectance of b-Si with 20 nm of Al_2O_3 (inset: zoomed view). The reflectance of random pyramids coated with 90-nm-thick Al_2O_3 film (dotted line) is shown as a reference.

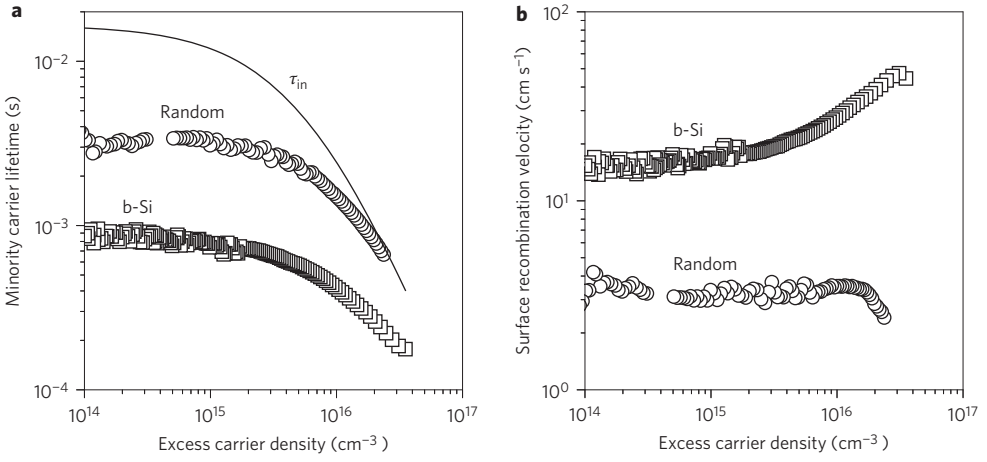

Figure 2 | Lifetimes and corresponding surface recombination velocities. a,**b**, Minority carrier lifetimes (**a**) and corresponding surface recombination velocities (**b**) as a function of minority carrier density. Values for the b-Si sample are shown as squares and values for the random pyramid sample are shown as circles. The solid line in **a** represents the intrinsic lifetime. Substrate resistivity is 2.6 ± 0.2 Ω cm in both samples.

b-Si fabrication is provided in the Methods. In principle, however, the results presented here should be independent of the b-Si fabrication method.

To passivate the b-Si we deposited a thin, 20 nm Al_2O_3 film, as described in the Methods. As a reference, we prepared samples with conventional micrometre-scale random pyramids and a 90-nm-thick Al_2O_3 antireflection (AR) coating. Figure 1b shows the measured reflectance of a b-Si wafer with and without the passivation film. Although extremely low reflectance is already achieved with the bare b-Si surface, the Al_2O_3 layer further reduces the reflectance to less than 1% between 300 and 1,000 nm (inset to Fig. 1b), which is the relevant wavelength range for solar cells. When compared to the random pyramid reference with a thick AR film, the benefit of b-Si becomes clear as in this material the reflectance is much lower at short (300–500 nm) and long (>700 nm) wavelengths. Moreover, it is well known that the positive impact of b-Si further increases when the light enters the cell from a wider angle[23]. The impact of the angle of incidence on the solar cell efficiency will be shown later in this Article.

The minority carrier lifetime is a material-quality-dependent parameter indicative of the time that it takes for the photogenerated charge carriers to recombine. It is a direct indicator of the maximum efficiency a solar cell can reach—the higher the lifetime the higher the cell efficiency. As a result, lifetime measurements give an effective carrier lifetime τ_{eff}, which is affected not only by the lifetime at the bulk but also by recombination at the wafer surfaces. Thus, it gives an idea about how well the surfaces are passivated. A direct indicator of surface passivation quality is the surface recombination velocity S_{eff}, which describes the velocity at which charge carriers reach the surface to recombine. When both surfaces are identical, the surface recombination velocity is related to the effective minority carrier lifetime through the relation

$$S_{eff} = \frac{W}{2}\left(\frac{1}{\tau_{eff}} - \frac{1}{\tau_{in}}\right) \quad (1)$$

where W is the wafer thickness, τ_{eff} the measured effective carrier lifetime, and τ_{in} is the intrinsic carrier lifetime according to

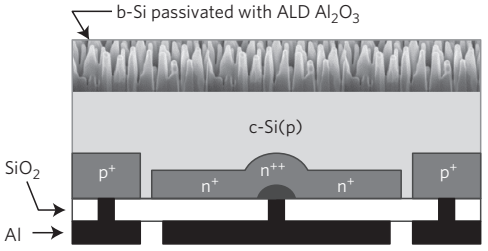

Figure 3 | Structure of the IBC cell. A thin Al_2O_3 layer is deposited on the nanostructured front surface. The solar cell fabrication process is presented in the Methods.

parametrization by Richter and co-authors[24]. As mentioned earlier, IBC cells require a low surface recombination velocity. Indeed, when efficiencies over 22% are targeted, the front surface recombination velocity needs to be below 30 cm s^{-1} (ref. 25).

Figure 2a shows a minority carrier lifetimes of ~1 ms in our b-Si samples, which corresponds to a surface recombination velocity S_{eff} of ~20 cm s^{-1} (Fig. 2b). These values are slightly higher than those we have reported previously and are probably caused by etching defects on the surface due to problems during the b-Si etching[17]. However, the values are still in the acceptable range from the solar cell point of view. In the reference samples the surface recombination velocities are as low as 3 cm s^{-1}.

b-Si solar cell with 22.1% efficiency

Figure 3 shows the cross-section of the IBC cell structure fabricated in this study. The collecting junction is on the back side, and no contacts (and thus no shadowing) are present on the front side. The surface area of the cells is 9 cm^2. The cells introduce selective emitters, meaning that there is a heavily doped region just beneath the contact to reduce the contact resistance and to hide the highly recombining contact from the rest of the junction. Four different emitter coverages were applied: 67, 75, 80 and 86%. Identical solar cells, but with a random pyramid texture, were fabricated as a reference. The details of the solar cell fabrication and characterization are provided in the Methods.

The current–voltage (*J*–*V*) and power–voltage (*P*–*V*) characteristics of the best b-Si solar cell are shown in Fig. 4a. These results were obtained for an emitter coverage of 80%. The photovoltaic parameter values are summarized in Table 1, where the results are directly compared with the reference counterpart (cell with random pyramid texture). Measurements from the b-Si solar cell show efficiencies over 22.1% (independently confirmed at Fraunhofer ISE CalLab PV Cells testing laboratory, as shown in the Supplementary Information), which is almost 4% absolute higher than values ever reached with any b-Si solar cell. In addition, this is the first time that the b-Si itself does not limit the solar cell efficiency, as the efficiency is comparable to the reference counterpart cell.

Table 1 | Photovoltaic results for the b-Si solar cell with emitter coverage of 80%.

Cell	J_{sc} (mA cm^{-2})	V_{oc} (mV)	FF (%)	η (%)
b-Si	42.2	665	78.7	22.1
Reference*	42.0	667	78.6	22.0

*As a comparison, values were taken from a random pyramid textured reference cell with the same emitter coverage.

The outstanding short-circuit current density J_{sc} of 42.2 mA cm^{-2}, as well as the good open-circuit voltage V_{oc} of 665 mV, prove the excellent front-surface passivation in the b-Si cell. This is also clearly seen from the external quantum efficiency (EQE) measurements in Fig. 4b, which show a flat behaviour in the short wavelength range with a value around 96%. In fact, the main difference with the reference counterpart cell is in the short wavelength range, where the reference cell clearly exhibits lower EQE values. This can be attributed to the much lower reflectance of the b-Si in the ultraviolet range. The similar EQE values in the infrared region (λ = 800–1,200 nm) indicate near identical rear surfaces on both the b-Si and reference cells, as can be expected.

Finally, due to the b-Si property of absorbing light with high acceptance angles, the high efficiency can be maintained independently of the direction of the incoming light (Fig. 5a). This is not the case with conventional AR coatings, which are only optimized for incident light perpendicular to the cell surface. This property has a high impact, especially in photovoltaics, because the Sun's radiation impinges solar cells from different angles throughout the day and through the year. Figure 5b shows the relative change in the photogenerated current with respect to normal illumination, for several incidence angles and considering both the reference and b-Si cells. For the b-Si cell, changes in the photogenerated current are under 1% for incidence angles below approximately 60°, whereas the reference counterpart loses up to nearly 4% in the same angle range. As a consequence, the quantity of energy delivered by the b-Si cell throughout the day/year also surpasses the energy produced by the reference solar cell. Figure 5c shows a simulation of the relative increase in produced

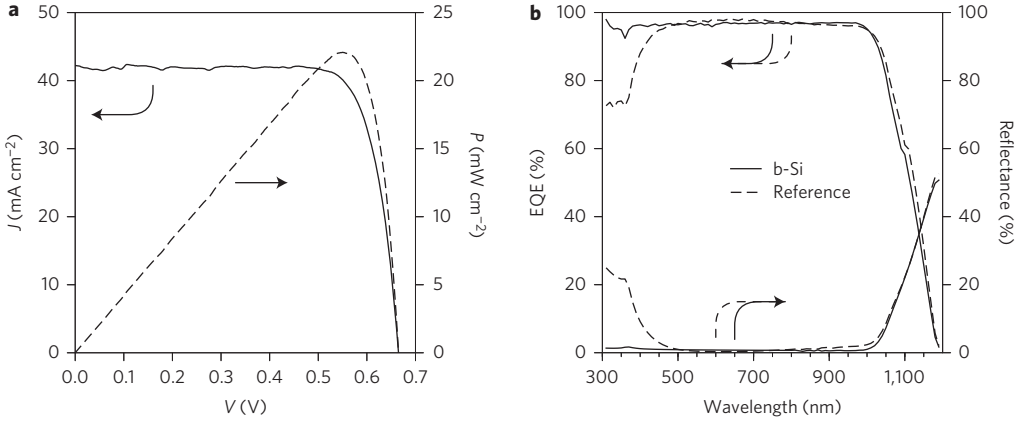

Figure 4 | EQE and *J*–*V* and *P*–*V* characteristics for the selected b-Si solar cell. a, *J*–*V* (solid line) and *P*–*V* (dashed line) characteristics of the b-Si cell with 80% emitter coverage. **b**, EQE and reflectance measurements for the best b-Si cell (solid lines) and the corresponding randomly texturized cell (dashed lines). EQE values were measured with bias light of 0.1 sun.

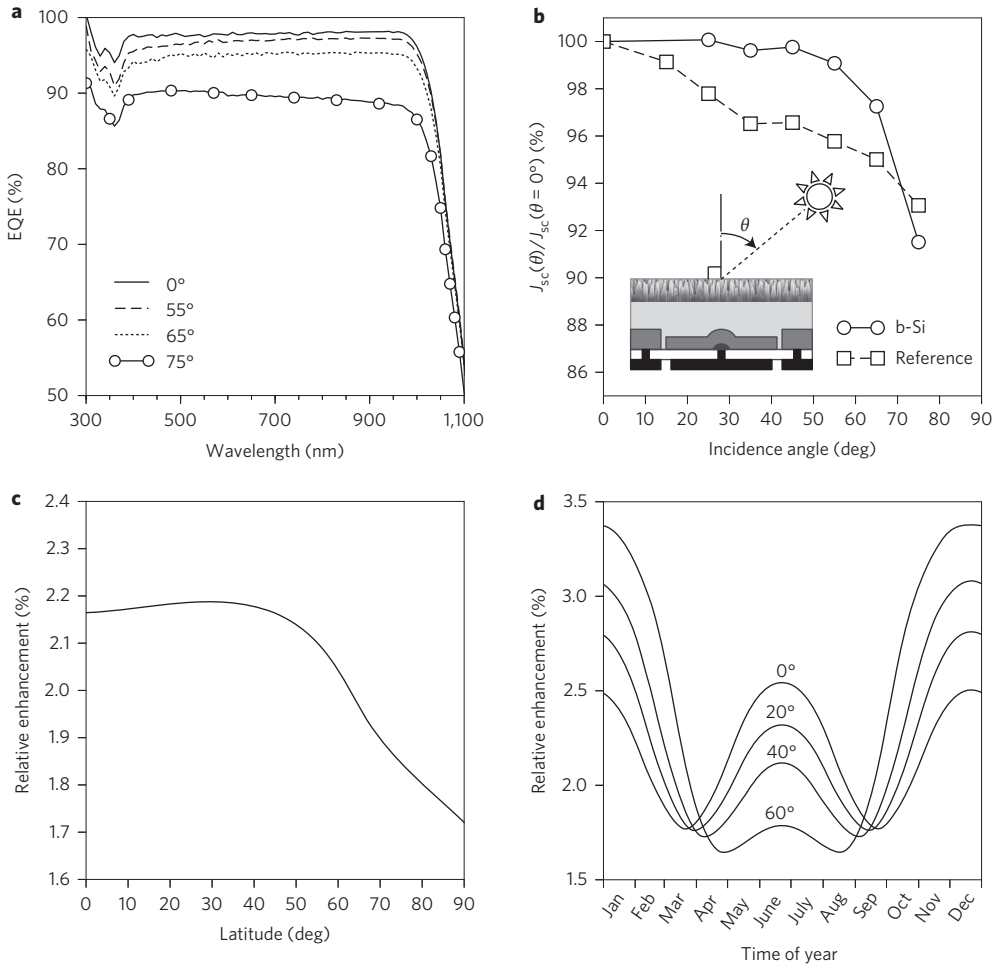

Figure 5 | Angle-dependent EQE and daily/yearly energy production enhancement. a, EQE of the b-Si cell for different angles of incidence. **b**, Relative photocurrent, with respect to photocurrent at normal incidence, for different light incidence angles for both the b-Si (circles) and reference (squares) solar cells. Light incidence angle θ is defined in the inset. **c**, Relative increase in total delivered energy throughout the year for the b-Si cell compared with the reference cell as a function of latitude and for optimally tilted cells. **d**, Daily relative increase, throughout the year, in the energy generated by the b-Si cell compared with the reference cell for different locations (60° latitude corresponds to Helsinki, 40° to Barcelona).

energy compared to the reference cell. For latitudes below 60° (Helsinki), relative increases greater than 2% are obtained over the year. This improvement is dependent on season. For instance, far from the equator, the increase is more important when insolation is lower (winter) and this asymmetry grows with latitude. As can be seen in Fig. 5d, at 40° of latitude the increase is more than 2.5% during the four months with less insolation. Details of the calculation procedure are provided in the Methods.

Our results show that the b-Si is no longer limiting the cell efficiency, so further improvements should be possible by improving the cell structure. For example, even higher efficiencies could be expected by optimizing the emitter coverage. Other improvements could be implemented in current IBC structures to increase fill factor (FF) and V_{oc} values. For instance, a thicker aluminium layer in fingers and busbars would reduce ohmic losses, thereby achieving higher FF values. Moreover, an optimized phosphorous doping profile in the low and high doped emitter regions might further decrease the emitter saturation current density, J_{oe}, increasing V_{oc} accordingly. Therefore, with realistic improved values of FF > 81% and V_{oc} > 675 mV, and assuming the excellent J_{sc} (42.2 mA cm^{-2}) value achieved in this study, efficiencies well beyond 23% might be expected soon. Furthermore, because Al_2O_3 passivation has been reported to work on n-type surfaces as well[26], we plan to use the approach reported here for an n-type IBC structure, which has even greater potential due to its higher bulk minority carrier lifetimes.

In summary, we have successfully developed a high-efficiency, p-type, b-Si IBC solar cell, with greater than 22% efficiency with a surface area of 9.0 cm^2. In the record cell we can use its optimal surface reflectance without affecting surface recombination, due to the outstanding surface passivation achieved with conformal ALD Al_2O_3. The use of a surface sensitive 280-μm-thick IBC structure proves that surface recombination, which has been hindering the use of b-Si in photovoltaics, is no longer a limiting factor. This should pave the way for even higher efficiencies in b-Si cells, not only in IBC structures but also in existing and new solar cell concepts.

Methods

Methods and any associated references are available in the online version of the paper.

Received 27 May 2014; accepted 25 March 2015; published online 18 May 2015

References

1. Clapham, P. B. & Hutley, M. C. Reduction of lens reflection by the 'moth eye' principle. *Nature* **3,** 281–282 (1973).

2. Zhu, J. *et al.* Optical absorption enhancement in amorphous silicon nanowire and nanocone arrays. *Nano Lett.* **9,** 279 (2008).
3. Garnett, E. & Yang, P. Light trapping in silicon nanowire solar cells. *Nano Lett.* **10,** 1082–1087 (2010).
4. Kelzenberg, M. D. *et al.* Enhanced absorption and carrier collection in Si wire arrays for photovoltaic applications. *Nature Mater.* **9,** 239–244 (2010).
5. Oh, J., Yuan, H-C. & Branz, H. M. An 18.2%-efficient black-silicon solar cell achieved through control of carrier recombination in nanostructures. *Nature Nanotech.* **7,** 743–748 (2012).
6. Zhu, J., Hsu, C-M., Yu, Z., Fan, S. & Cui, Y. Nanodome solar cells with efficient light management and self-cleaning. *Nano Lett.* **10,** 1979–1984 (2010).
7. De Boer, M. J. *et al.* Guidelines for etching silicon MEMS structures using fluorine high-density plasmas at cryogenic temperatures. *J. Micromech. Microeng.* **11,** 385–401 (2002).
8. Gesemann, B., Wehrspohn, R., Hackner, A. & Müller, G. Large-scale fabrication of ordered silicon nanotip arrays used for gas ionization in ion mobility spectrometers. *IEEE Trans. Nanotechnol.* **10,** 50–52 (2011).
9. Hoyer, P., Theuer, M., Beigang, R. & Kley, E-B. Terahertz emission from black silicon. *Appl. Phys. Lett.* **93,** 091106 (2008).
10. Sainiemi, L. *et al.* Rapid fabrication of high aspect ratio silicon nanopillars for chemical analysis. *Nanotechnology* **18,** 505303 (2007).
11. Huang, Z. *et al.* Microstructured silicon photodetector. *Appl. Phys. Lett.* **89,** 033506 (2006).
12. Ivanova, E. P. *et al.* Bactericidal activity of black silicon. *Nature Commun.* **4,** 2838 (2013).
13. Jeong, S., McGehee, M. D. & Cui, Y. All-back-contact ultra-thin silicon nanocone solar cells with 13.7% power conversion efficiency. *Nature Commun.* **4,** 2950 (2013).
14. Zhong, S. *et al.* Influence of the texturing structure on the properties of black silicon solar cell. *Sol. Energ. Mater. Sol. Cells* **108,** 200–204 (2013).
15. Koynov, S., Brandt, M. S. & Stutzmann, M. Black multi-crystalline silicon solar cells. *Phys. Status Solidi RRL* **1,** R53–R55 (2007).
16. Hoex, B., Schmidt, J., Pohl, P., van de Sanden, M. C. M. & Kessels, W. M. M. Silicon surface passivation by atomic layer deposition Al_2O_3. *J. Appl. Phys.* **104,** 044903 (2008).
17. Repo, P. *et al.* Effective passivation of black silicon surfaces by atomic layer deposition. *IEEE J. Photovolt.* **3,** 90–94 (2013).
18. Otto, M. *et al.* Extremely low surface recombination velocities in black silicon passivated by atomic layer deposition. *Appl. Phys. Lett.* **100,** 191603 (2012).
19. Neuhaus, D. & Münzer, A. Industrial silicon wafer solar cells. *Adv. Optoelectron.* **2007,** 24521 (2007).
20. Halbwax, M. *et al.* Micro and nano-structuration of silicon by femtosecond laser: application to silicon photovoltaic cells fabrication. *Thin Solid Films* **516,** 6791–6795 (2008).
21. Toor, F., Branz, H. M., Page, M. R., Jones, K. M. & Yuan, H-C. Multi-scale surface texture to improve blue response of nanoporous black silicon solar cells. *Appl. Phys. Lett.* **99,** 103501 (2011).
22. Sainiemi, L. *et al.* Non-reflecting silicon and polymer surfaces by plasma etching and replication. *Adv. Mater.* **23,** 122–126 (2011).
23. Huang, Y-F. *et al.* Improved broadband and quasi-omnidirectional anti-reflection properties with biomimetic silicon nanostructures. *Nature Nanotech.* **2,** 770–774 (2007).
24. Richter, A., Glunz, S. W., Werner, F., Schmidt, J. & Cuevas, A. Improved quantitative description of Auger recombination in crystalline silicon. *Phys. Rev. B* **86,** 165202 (2012).
25. Carrio, D. *et al.* Rear contact optimization based on 3D simulations for IBC solar cells with point-like doped contacts. *Energy Procedia* **55,** 47 (2014).
26. Hoex, B., van de Sanden, M. C. M., Schmidt, J., Brendel, R. & Kessels, W. M. M. Surface passivation of phosphorus-diffused n^+-type emitters by plasma-assisted atomic-layer deposited Al_2O_3. *Phys. Status Solidi RRL* **6,** 4–6 (2012).

Acknowledgements

This work was supported by the network 'Nanophotonics for Energy Efficiency' (grant agreement no. 248855), the Effinano-project (funded by the School of Electrical Engineering at Aalto University) and the Tekes-funded project PASSI. The authors acknowledge The Centre for Research in NanoEngineering (CRnE) and Aalto University Micronova Nanofabrication Centre for providing facilities. The authors thank T. Trifonov for help and comments on performing reflectance measurements and V. Vähänissi for providing valuable comments regarding writing the manuscript.

Author contributions

H.S. and R.A. conceived and designed the experiments. P.R., G.G., P.O. and E.C. performed the experiments. P.O. and H.S. analysed the data. M.G. performed the angle-dependent simulations. H.S. wrote the paper. All authors discussed the results and commented on the manuscript.

Additional information

Supplementary information is available in the online version of the paper. Reprints and permissions information is available online at www.nature.com/reprints. Correspondence and requests for materials should be addressed to H.S.

Competing financial interests

The authors declare no competing financial interests.

Methods

Sample fabrication. The b-Si was etched using a cryogenic inductively coupled plasma reactive-ion etching process (Plasmalab System 100, Oxford Instruments) at −120 °C using SF_6 and O_2 as the etching gases. For the lifetime tests, starting wafers were high-quality 4-inch p-type Float Zone silicon ⟨100⟩ with a resistivity of 2.6 ± 0.2 Ω cm and thickness of 280 ± 20 μm. Some wafers were b-Si etched on both sides, and the others were anisotropically etched using a mix of tetramethylammonium hydroxide (TMAH), isopropanol (IPA) and deionized water (320 ml:350 ml:3,300 ml) at 80 °C for 70 min to form random pyramids on both wafer surfaces. After etching, the wafers were RCA cleaned and HF-dipped, followed by surface passivation with 20- and 90-nm-thick ALD Al_2O_3 in the b-Si etched and random textured samples, respectively. The ALD process was carried out in all cases using TMA as the aluminium source and H_2O as the oxidant. The surface passivation of the b-Si wafers was activated with a 30 min anneal at 400 °C in N_2. The random textured wafers were annealed using a forming gas atmosphere (95% N_2/5% H_2) at 400 °C for 10 min.

The b-Si IBC and reference solar cells with random pyramids were fabricated on high-quality 4-inch p-type Float Zone silicon ⟨100⟩ with a resistivity of 2.4 ± 0.2 Ω cm and thickness of 280 ± 20 μm. The main fabrication steps were as follows. (1) Boron and phosphorous diffusions, using solid dopant sources to form p^+ (base contacts), n^+ (low doped emitter) and n^{++} (high doped emitter) regions, respectively, were patterned using standard photolithography. (2) b-Si solar cells or random textured reference cells were surface passivated with 20 nm or 90 nm ALD Al_2O_3 films, respectively. (3) A back-reflector scheme was created consisting of a thermal SiO_2(110 nm)/Al(3 μm) stack. Al_2O_3 deposition on the b-Si cells was carried out using TMA and H_2O as the precursors, and the passivation was activated with a 30 min anneal at 400 °C in N_2. The ALD process and annealing stage for the reference IBC cells were identical to those used for the reference lifetime samples already described. Four solar cells with different emitter coverages (area of the emitter relative to the total rear surface area) of 67, 75, 80 and 86% were fabricated on each wafer. Device areas (3 cm × 3 cm) were clearly defined by light windows in an electron-beam evaporated aluminium metallization layer (thickness of 0.4 μm) in the front side.

Sample characterization. Lifetimes as a function of minority carrier density of the symmetrically etched b-Si and random pyramid textured samples were measured with a quasi-steady-state photoconductance method (Sinton Instruments WCT-120). The corresponding surface recombination velocities were calculated as described in the main text. Solar cells were measured using a solar simulator (ORIEL 94021A) under standard test conditions (AM1.5G 1 kW m^{-2} solar spectrum $T = 25$ °C). Only the nanostructured solar cell efficiency was independently confirmed by the Fraunhofer ISE CalLab PV Cells certified photovoltaics testing laboratory. Calibration of the ORIEL simulator used may differ slightly. Reflectance measurements were carried out using a UV-vis-NIR spectrometer with an integrating sphere (Shimadzu 3600) in the 300–1,200 nm wavelength range, and EQE characterization was performed using a solar cell quantum efficiency measurement system (QEX10) with a beam spot area of ~2 cm × 2 cm and 0.1 sun of bias light. Angle-dependent EQE measurements were carried out with the same instrument but using a small beam light size (0.5 cm × 1 cm) to ensure that the whole light spot impinged into the active solar cell area.

Relative improvement calculation. We calculated the relative improvement in the performance of a b-Si and a reference textured cell with different angles of incidence during the day and over a year. The calculation took into account only direct Sun radiation (diffuse and albedo components were not considered). Calculations were performed at different latitudes for a fixed flat panel optimally tilted for that particular latitude. A Sun position algorithm[27] (giving the Sun vector at any time with an accuracy of ~1°) was used. Local atmospheric effects were irrelevant as the calculation was restricted to relative improvements. Nevertheless, in the calculations we estimated the irradiance on the Earth's surface through the year, considering clear sky conditions and the air mass. The apparent solar dawn and dusk on the tilted plane of the photovoltaic module were considered. To determine the output power, the short-circuit current at a given time was scaled from the 1 sun measured value taking into account the experimentally measured angle dependence. Finally, the maximum output power was determined and integrated on a daily and yearly basis.

References

27. Masters, G. M. *Renewable and Efficient Electric Power Systems* (Wiley, 2004).